



The asymmetric impacts of ENSO modoki on boreal winter climate over the Pacific and its rim

Linqiang He¹ · Xin Hao^{1,2} · Tingting Han^{1,2}

Received: 24 October 2019 / Accepted: 24 July 2020 / Published online: 23 September 2020
© Springer-Verlag GmbH Germany, part of Springer Nature 2020

Abstract

The El Niño–Southern Oscillation (ENSO) Modoki phenomenon has a substantial influence on regional climate. In this study, the results derived from observational and reanalyzed datasets show that the boreal winter climate anomalies over the Pacific and its rim in the different phases of ENSO Modoki are asymmetric during 1979–2017. During El Niño Modoki, an upper-level zonal “convergence–divergence–convergence” anomaly occurred in the Walker circulation over the Pacific sector, associated with anomalous ascending (descending) in the central side (both sides), leading to a wet “boomerang” pattern of rainfall anomalies in the tropical Pacific Ocean. Consequently, a drier winter occurred in Philippines, and warming and drying occurred in western Australia and northern South America. Meanwhile, a dipolar pattern with the wet south and the dry north in the United States occurred, accompanied by a Pacific/North American-like teleconnection. During La Niña Modoki, a roughly reversed Walker circulation anomaly and deeper Hadley circulation anomalies were associated with the strong air–sea feedback, which caused stronger rainfall anomalies in the Pacific Ocean. On land, anomalies of surface temperature and rainfall over the tropical Pacific Rim were more intense compared with El Niño Modoki. However, owing to the lack of a Pacific/North American anomaly, fewer anomalies occurred over the mid-latitude North America. In numerical experiments, the response to the different phases of ENSO Modoki basically reproduces the asymmetric climate anomalies in boreal winter, further confirming that the asymmetry can be partly attributed to tropical sea surface temperature anomalies.

Keywords ENSO modoki · Boreal winter climate · Asymmetry · Air–sea feedback

1 Introduction

El Niño Modoki is known as a coupled ocean–atmosphere phenomenon associated with the tripole pattern of sea surface temperature (SST) anomalies in the equatorial Pacific, which is different from the canonical El Niño (Ashok et al.

2007; Weng et al. 2007). When El Niño Modoki occurs, warm SST anomalies are observed over the central equatorial Pacific and cold SST anomalies occur in its east and west sides, and the opposite pattern is detected during La Niña Modoki. Many previous studies have discussed the formation and cycle of the canonical El Niño–Southern Oscillation (ENSO), including the mechanism of positive feedback (Bjerknes 1969), the theory of trade winds (Wyrski 1975), the unstable wave theory of air–sea interaction (Philander et al. 1984), a delayed action oscillator view (Suarez and Schopf 1988; Battisti and Hirst 1989), and recharge paradigm theory in the late 1990s (Jin 1997a, b). The understanding of the physical mechanisms of the canonical ENSO has gradually improved, and the mechanisms have also been verified with large observational datasets and modeling experiments. The impact of canonical ENSO events on the global climate is always a concern (Brönnimann 2007; Mariotti 2007), and its remarkable effects have been applied widely in short-term climate predictions (Xu et al. 2005).

Electronic supplementary material The online version of this article (<https://doi.org/10.1007/s00382-020-05395-z>) contains supplementary material, which is available to authorized users.

✉ Xin Hao
haoxlike91@163.com

¹ Collaborative Innovation Center on Forecast and Evaluation of Meteorological Disasters/Key Laboratory of Meteorological Disaster, Ministry of Education, Nanjing University of Information Science and Technology, Nanjing 210044, China

² Nansen-Zhu International Research Center, Institute of Atmospheric Physics, Chinese Academy of Sciences, Beijing 100029, China

By contrast, research on the evolution of ENSO Modoki and associated climate change is still ongoing. Previous studies have shown that ENSO Modoki is likely to be an event induced by local air–sea coupling (Kao and Yu 2009; Yu et al. 2010). Ashok et al. (2007) found that the flattening thermocline resulting from weakening equatorial easterlies leads to more El Niño Modoki events. Jadhav et al. (2015) and Kug et al. (2009) also found that zonal advection, including zonal wind and average zonal SST gradient, plays an important role in the development of El Niño Modoki. Nevertheless, Yu et al. (2010) argued that the role of zonal advection only works when the central equatorial SST anomalies are established. Moreover, Yu and Kim (2011) also suggested that El Niño Modoki may be related to the force of Asian–Australian monsoon and extratropical atmosphere, that is, sea-level pressure (SLP) interannual variability over the subtropical and extratropical sea influenced by the monsoon may cause anomalous trade winds and further trigger the warm SST anomalies in the central equatorial Pacific.

Recently, the interaction between ENSO Modoki events and regional climate has been drawn much attention due to its multifaceted effects over East Asia (Feng et al. 2011; Kim et al. 2012), Southeast Asia (Feng et al. 2010; Salimun et al. 2014), North America (Yu et al. 2017; Weng et al. 2009), South America (Tedeschi et al. 2013; Samir et al. 2015), and the African continent (Preethi et al. 2015). On the one hand, since El Niño Modoki was proposed, some researchers have focused on the comparison of the climate response to the ENSO Modoki with the response to the canonical ENSO and proved the existing distinction. For example, an anomalous anticyclone occurs over South China Sea during El Niño Modoki while it occurs over the Philippine Sea during El Niño, which leads to opposite precipitation anomalies in Southeast Asia (Weng et al. 2009; Feng et al. 2010). A significant rainfall decrease is mainly observed in austral winter and summer over the northern, central, and western Colombia during El Niño and El Niño Modoki, while the opposite impact occurs in some localities during austral spring and autumn (Samir et al. 2015). During El Niño Modoki, the northward-shifted Intertropical Convergence Zone (ITCZ) transports moisture to southwestern North America, leading to a seesaw pattern with a dry north and wet south, while the western United States is wet and its moisture mainly comes from the southward-shifted polar front jet that moves southward when El Niño occurs (Weng et al. 2009). In addition, the difference between the impacts of El Niño and El Niño Modoki on subdaily extreme precipitation occurrences in the United States was investigated by Yu et al. (2017).

On the other hand, many studies have indicated that there are regional asymmetric features of seasonal climate anomalies during different phases of ENSO Modoki (Karori et al. 2013; Cai et al. 2010). Karori et al. (2013) found an asymmetric relationship between ENSO Modoki events and

boreal summer rainfall over Southeast China, which may be caused by different spatial patterns of SST anomalies. Specifically, El Niño Modoki has a noticeable positive correlation with summer rainfall over South China, whereas La Niña Modoki has a positive influence on summer rainfall over the Yangtze River. Cai et al. (2010) revealed that austral summer precipitation in southeast Queensland increased with La Niña Modoki amplitude, which is statistically significant compared with the decrease in El Niño Modoki-induced rainfall, which has no evident correlation with its amplitude. During boreal winter, the asymmetric interactions between ENSO Modoki events and atmospheric teleconnection or coupled ocean–atmosphere phenomena also have to be taken into account. ENSO Modoki can induce circulation anomalies, such as the Arctic Oscillation (AO), which are more intense during El Niño Modoki because of the difference in background fields (Cheng et al. 2019). Wang et al. (2017) suggested that a negative phase of the North Atlantic Oscillation (NAO) occurs during El Niño Modoki boreal winter, bringing about low temperatures over Northeast China; although La Niña Modoki occurs accompanied by a positive phase of the NAO, the temperature anomalies are not significant due to the spatial shifting of the NAO structure.

Over the past two decades, the frequency and duration of ENSO Modoki events have far exceeded that of canonical ENSO events (Ashok et al. 2007; Marathe et al. 2015; Freund et al. 2019). On the basis of the asymmetric atmospheric circulation anomalies during different phases of ENSO Modoki, the relationship between ENSO Modoki events and boreal winter climate may show distinct features, which remain unclear. Therefore, this study investigates the possible asymmetry between ENSO Modoki events and winter climate over the Pacific Ocean and its rim and further explores the corresponding physical mechanism. This study contributes to the understanding and prediction of the effect of ENSO Modoki events on regional climate change.

The remainder of this paper is structured as follows. Section 2 describes the data, methods, and model experiments we adopted. In Sect. 3, winter climate anomalies during ENSO Modoki are presented. Section 4 presents the possible mechanism of the asymmetry through observational analysis and Sect. 5 shows the results of model experiments to confirm the observational results. Finally, section 6 provides a summary.

2 Data, methods and model experiment

2.1 Data and methods

The datasets used in this study are monthly SST from the Hadley Centre Global Sea Ice and Sea Surface Temperature

with $1^\circ \times 1^\circ$ horizontal resolution (HadISST, Rayner et al. 2003), monthly precipitation rate from the Global Precipitation Climatology Project (GPCP) Version 2.3 with $2.5^\circ \times 2.5^\circ$ horizontal resolution (Adler et al. 2018), monthly surface temperature from the Climatic Research Unit, University of East Anglia (CRU TS) Version 3.23 with $0.5^\circ \times 0.5^\circ$ horizontal resolution (Harris and Jones 2015), and some monthly meteorological variables from the ERA-Interim Reanalysis with $1^\circ \times 1^\circ$ horizontal resolution (Berrisford et al. 2011). Here we focus on the boreal winter, which consists of December to February of the following year. For example, the boreal winter of 1990 refers to the 3-month average of 1990–12, 1991–01, 1991–02. All anomalies mentioned are deviations from the winter climatological mean of 1980–2010. The composite difference is presented as the average of anomalies during El Niño Modoki and La Niña Modoki. All datasets used here are linearly detrended. The significance of the regression and composite analysis is obtained by a two-tailed Student’s *t* test.

The ENSO Modoki Index (EMI; Ashok et al. 2007) from the Japan Agency for Marine–Earth Science and Technology (JAMSTEC; Fig. 1) is adopted in this study. The monthly EMI can be obtained from https://www.jamstec.go.jp/frsgc/research/d1/iod/modoki_home.html.en. Cases with a normalized winter EMI equal to or greater (less) than 0.7 (−0.7) are defined as an El Niño Modoki (La Niña Modoki) event (Ashok et al. 2007; Samir et al. 2015). Note, we removed the years 1997 and 2015, which should be canonical El Niño events. One the basis of the above criterion, we identify ten typical boreal winter El Niño Modoki events in 1979, 1986, 1990, 1991, 1992, 1994, 2002, 2004, 2009, and 2014, and nine typical boreal winter La Niña Modoki events in 1983, 1988, 1998, 1999, 2000, 2007, 2008, 2010, and 2011. The SST anomalies of selected ENSO Modoki events shown in Fig. S1 are concentrated on the central equatorial Pacific Ocean which is the distinctive feature of ENSO Modoki.

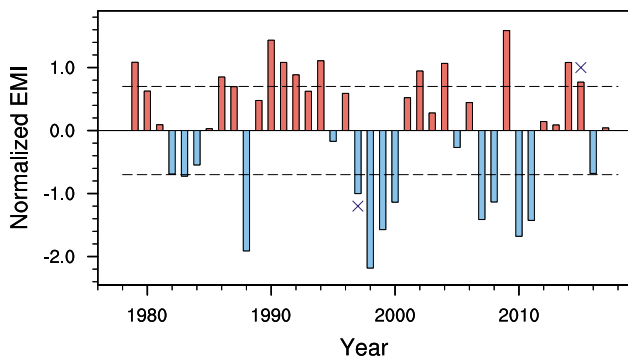


Fig. 1 Normalized Dec–Jan–Feb (DJF) time series of the EMI. Dashed lines indicate the reference of ± 0.7 and crosses denote the year of canonical El Niño events

According to Sun et al. (2011), the vertically integrated horizontal moisture flux \bar{Q} can be expressed as.

$$\bar{Q} = -\frac{1}{g} \int_{P_s}^{P_t} q \bar{V} dp = -\frac{1}{g} \int_{P_s}^{P_t} (uq\vec{i} + vq\vec{j}) dp \tag{1}$$

Here *g* is the gravity acceleration with a value of 9.8 (ms⁻²), *P_s* is the surface pressure, *P_t* is the pressure at 300 hPa, *q* is the specific humidity, and *u* and *v* are the zonal and meridional velocity, respectively. The horizontal moisture flux divergence at a single grid can be calculated as.

$$-\frac{1}{g} \int_{P_s}^{P_t} \nabla \cdot q \bar{V} dp = -\frac{1}{g} \int_{P_s}^{P_t} \left(\frac{\partial qu}{\partial x} + \frac{\partial qv}{\partial y} \right) dp \tag{2}$$

2.2 Model experiment

Using the Community Earth System Model (CESM; Gent et al. 2011) Version 1.2.2, we examine the impacts of ENSO Modoki on boreal winter climate change over the Pacific and its rim. Specifically, we run a standalone atmospheric component with prescribed SSTs (F_20000_CAM5). A $1.9^\circ \times 2.5^\circ$ finite volume grid resolution is used for the atmospheric and land components and a 1° displaced pole grid resolution is used for the oceanic and ice components (1.9x2.5_gxlv6). The prescribed SSTs include three different scenarios (Table 1). Here monthly climatological SST is a monthly average over the period of 1982–2001, and the ENSO Modoki SST anomalies over the tropical Pacific Ocean ($30^\circ S - 30^\circ N, 120^\circ E - 70^\circ W$) are added to the monthly climatological SST in November, December, January, and February. Each run is continuously integrated for 35 years and we take average of the last 30 years as the results. Therefore, the simulated climate responses to ENSO Modoki are the differences between the CENSO_warm (CENSO_cold) runs and CENSO_control runs.

Table 1 Prescribed SST in model experiments

Experiment Name	Experiment Content
CENSO_control	Climatological monthly SST
CENSO_warm	Climatological monthly SST + El Niño Modoki SST anomalies
CENSO_cold	Climatological monthly SST + La Niña Modoki SST anomalies

3 Winter climate anomalies during ENSO Modoki

3.1 Relationship between ENSO Modoki and winter climate

Several studies have revealed the impact of ENSO Modoki event on regional winter climate (Tedeschi et al. 2013; Karori et al. 2013; Preethi et al. 2015). To verify the relationship between the winter climate over the Pacific Rim and ENSO Modoki, we conduct regression analysis of the surface air temperature (SAT) and precipitation rate anomalies with the normalized EMI. Using the CRU TS dataset, we find that ENSO Modoki events are positively correlated with winter SAT anomalies over most regions of the Pacific Rim, including northwestern and southeastern China, southern Kamchatka, southern Alaska, the west coast of the United States, northern South America, and

northeastern and northwestern Australia (Fig. 2a). Meanwhile, a negative correlation between ENSO Modoki and SAT anomalies is observed over southern South America and the Gulf Coast (Fig. 2a). On the basis of the GPCP precipitation rate, rainfall anomalies also show an obvious change over the Pacific and its rim. Clearly, a zonal tripolar pattern of “negative–positive–negative” precipitation anomalies occur in the equatorial Pacific (Fig. 2c). Furthermore, a dipolar pattern with negative anomalies over the western and central Pacific and positive anomalies over the eastern Pacific are observed in the extra-equatorial regions. On land, ENSO Modoki events are positively correlated with boreal winter precipitation anomalies over the coast of Alaska and southwestern North America, whereas negative linear regression coefficients are seen over most regions of Southeast Asia, western Kamchatka, the Great Lakes region, northern and northwestern South America, and western Australia.

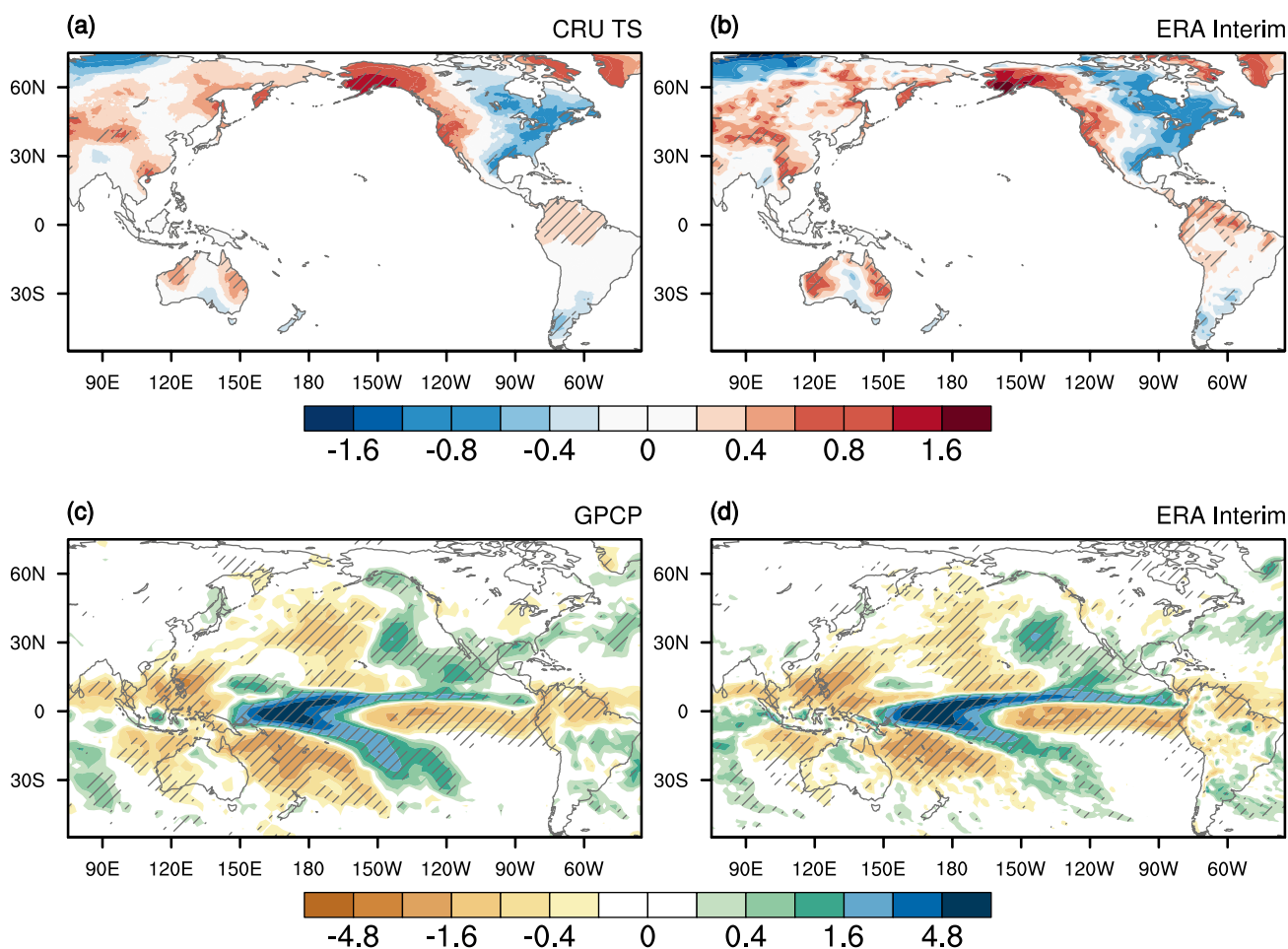


Fig. 2 Regression patterns of boreal winter SAT anomalies from the CRU (a) and ERA Interim (b) datasets, and precipitation rate anomalies from the GPCP (c) and ERA Interim (d) datasets with the nor-

malized EMI during 1979–2017. Slant hatching denotes the 90% confident level from a Student's *t* test

The regressed results of SAT and precipitation anomalies from the ERA-Interim dataset are consistent with the results obtained from the observational datasets (Fig. 2b,d). Owing to the higher horizontal resolution, “boomerang” patterns (Weng et al. 2009) of rainfall anomalies in the Pacific Ocean are clearer in Fig. 2d. This similarity indicates that the relationship between ENSO Modoki and the monthly SAT is reliable over the Pacific Rim.

3.2 Asymmetric winter climate anomalies during the different phases

Figure 3a, b presents the boreal winter composite differences of SAT during the different phases of ENSO Modoki, and the asymmetry can be seen in Fig. 3c. During El Niño Modoki, warm anomalies are observed in northwestern Australia, and northwestern and northern South America (Fig. 3a), whereas La Niña Modoki occurs with cold anomalies in the western Marine Continent, the western coast of the United States, the

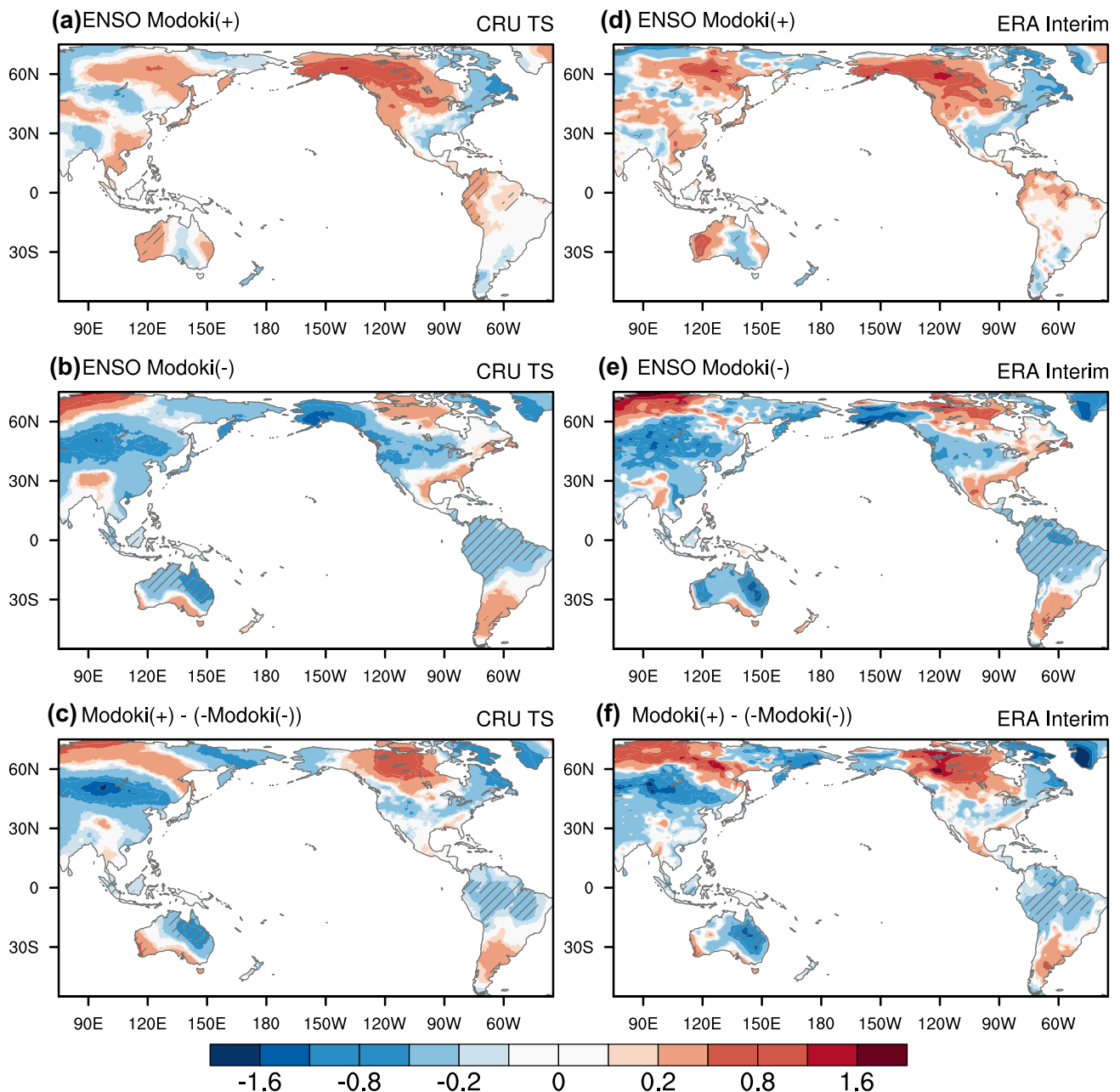


Fig. 3 Composite DJF SAT anomalies (unit: °C) from the CRU (left panel) and ERA-Interim (right panel) datasets during 1979–2017. (c) and (f) show the asymmetry between a and b, c and d, respectively. Slant hatching denotes the 90% confident level from a Student’s *t* test

Caribbean coast, and the entire north of South America and north of Australia (Fig. 3b). Notably, a zonal tripolar pattern with “positive–negative–positive” anomalies is observed in Australia during El Niño Modoki (Fig. 3a), whereas a meridional dipolar pattern with “positive–negative” anomalies occurs in La Niña Modoki (Fig. 3b). The asymmetric difference between El Niño Modoki and La Niña Modoki (El Niño Modoki $- (-1 \times \text{La Niña Modoki})$) shows that stronger SAT anomalies occur over the western Marine Continent, northeastern Australia, and northern South America during

La Niña Modoki (Fig. 3c). The results from the ERA-Interim dataset capture similar SAT anomaly signals (Fig. 3d–f).

Using the GPCP dataset, composites of precipitation anomalies are shown in Fig. 4a, b. The opposite patterns of precipitation anomalies over the Pacific Ocean are observed during different phases, which is characterized by a “boomerang” pattern extending from the western equatorial Pacific to the central North Pacific/South Pacific Convergence Zone, and another one extending from the central equatorial Pacific to the eastern North Pacific/

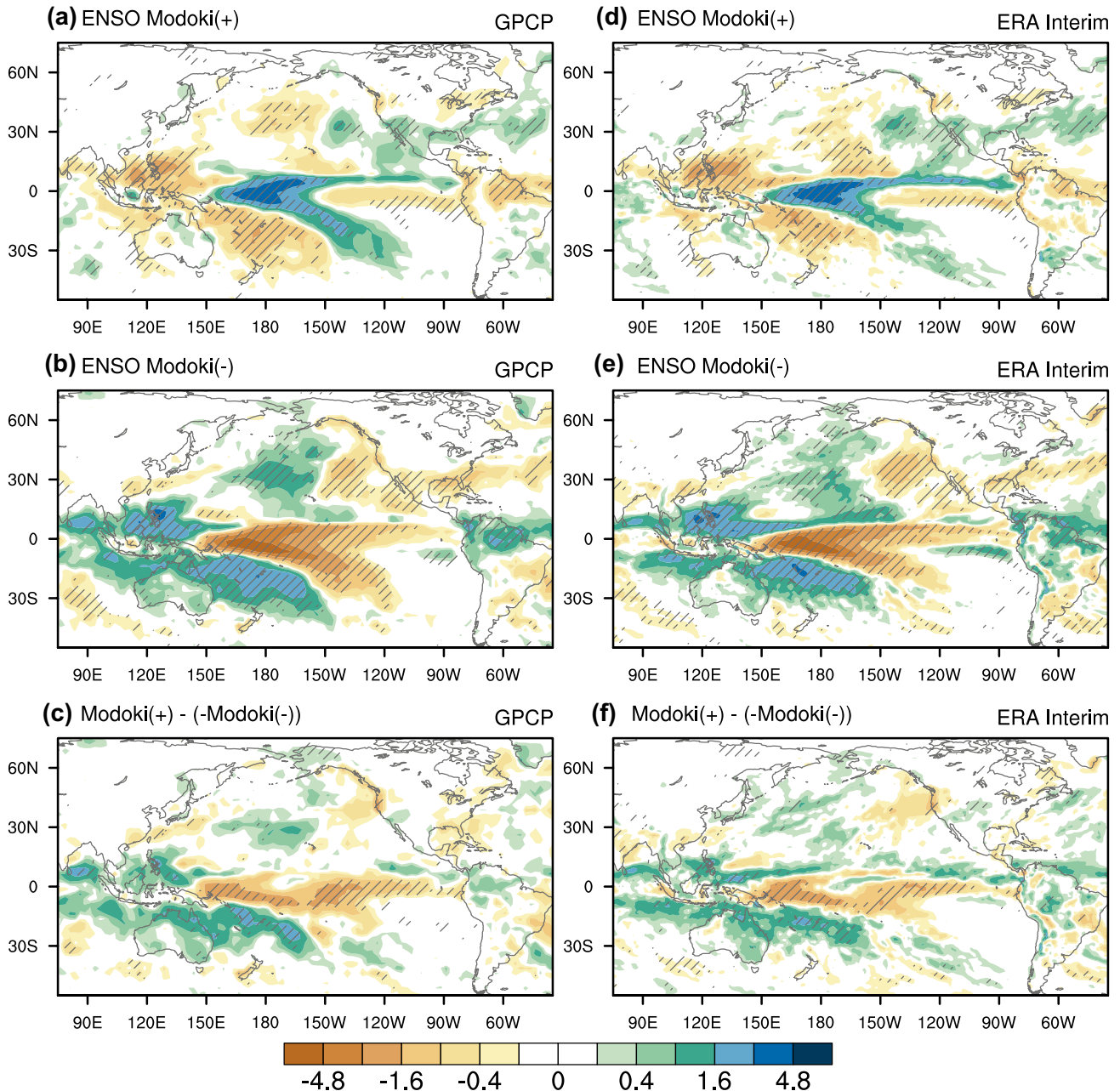


Fig. 4 The same as Fig. 3, but for precipitation rate anomalies (unit: mm day⁻¹) from the GPCP (left panel) and ERA Interim (right panel) datasets

central tropical South Pacific (Fig. 4a, b). The multiple “boomerang” patterns are significantly intensified in La Niña Modoki events, although rainfall anomalies over the eastern equatorial Pacific are slightly weaker compared with El Niño Modoki (Fig. 4c). On land, during El Niño Modoki, a decrease in rainfall occurs in the northern Maritime Continent, northern South America, and southwestern Australia (Fig. 4a). A meridional seesaw of wet and dry conditions in the southern and northern United States is detected only in El Niño Modoki, whereas a similar seesaw in the Philippines is robust during different phases. During La Niña Modoki, more precipitation anomalies are observed over tropical land, including drying in southwestern China and the Gulf Coast, and wetting in northeastern Australia and Venezuela, while anomalies over extratropical land are absent (Fig. 4b). Composites based on the ERA-Interim dataset (Fig. 4d–f) show the same pattern of boreal winter precipitation anomalies during different phases.

3.3 Associated circulation anomalies during the different phases

Changes in the large-scale atmospheric circulation could alter the intensity and likelihood of climate change (Screen 2014; Hao and He 2017). Further, we investigate the atmospheric circulation anomalies during different phases. Accompanied by the warming in the central equatorial Pacific during El Niño Modoki, positive 500 hPa geopotential height anomalies form over the entire equatorial Pacific and negative anomalies occur in the mid-latitudes of the North Pacific (Fig. 5a). Meanwhile, an anomalous high belt around 60°N contains two centers, with some degree of symmetry about the Bering Sea. A high-pressure anomaly over northwestern North America and two low-pressure anomalies over the North Pacific and western subtropical Atlantic Ocean resemble the Pacific–North American (PNA) pattern, favoring a meridional seesaw of wet and dry conditions over the southern and northern United States (Fig. 4a). This sign-alternating geopotential height anomaly in the Northern Hemisphere indicates that a meridional wave trains extend from the tropical central Pacific to high latitudes, implying a robust interaction between the tropics and extratropics (Fig. 5a).

In the lower troposphere, El Niño Modoki occurs with anomalous cyclonic winds over the mid-latitudes of the North Pacific (Fig. 5c). Water vapor flux (WVF) divergence anomalies on the western flank of the anomalous cyclone lead to less rainfall, which is opposite on its eastern side. Accompanied by this anomalous cyclone, southwesterly anomalies transport moisture from the ITCZ to the western coast of North America (Fig. 5e), which is consistent with the results in Weng et al. (2009). Meanwhile, easterly anomalies (Fig. 5c) in the northern flank of the anomalous western Atlantic cyclone (Fig. 5c)

can bring moisture to the Gulf Coast of Mexico (Fig. 5e). Both of the two water vapor channels provide moisture for boreal winter rain over the southern United States (Fig. 4a). In contrast, southwesterly anomalies in the southern flank of the western Atlantic anomalous cyclone transport the moisture away (Fig. 5e), causing less rainfall over northeastern South America (Fig. 4a). In addition, anomalous anticyclonic winds and WVF divergence dominate the Maritime Continent and Great Lakes, causing obvious dry anomalies there. During La Niña Modoki, the reversed 500 hPa geopotential height (Fig. 5b), SLP (Fig. 5d), and WVF (Fig. 5f) anomalies are stronger over the tropical Pacific and mid-latitudes of the North Pacific, causing more robust changes in rainfall in the corresponding regions (Figs. 3 and 4). However, the teleconnection between La Niña Modoki and North America is weaker (Fig. 5b) compared with El Niño Modoki (Fig. 5a).

4 Possible mechanism of the asymmetry

4.1 SST anomalies

Figure 6 shows the composites of SST anomalies from the HadISST dataset during different phases of ENSO Modoki. The tripolar pattern over the equatorial Pacific during El Niño Modoki is basically opposite to that during La Niña Modoki (Tedeschi et al. 2013; Karori et al. 2013). However, the intensity and scope of the SST anomalies are distinct. Compared with the anomalies in El Niño Modoki boreal winter (Fig. 6a), stronger cold anomalies occur in the equatorial central and eastern Pacific (Fig. 6c) and the meridional scope of the cold SST anomalies is larger in La Niña Modoki boreal winter (Fig. 6b), which may be attributed to the enhanced trade winds and thus strengthened upwelling and meridional currents, causing SST anomalies to more effectively spread away from the Equator (Zhang et al. 2009, 2013). Meanwhile, during La Niña Modoki, warm anomalies, stretching from Southeast Asia northward to about 40°N in the western North Pacific, are stronger than that in El Niño Modoki events, particularly in the central North Pacific (Fig. 6c). The equatorial cold tongue in the eastern Pacific Ocean is only observed in El Niño Modoki boreal winter. In addition, notable differences in the SST anomalies are observed in the Indo-Pacific warm pool, which may cause different impacts over East Asia, Southeast Asia, and Australia (Wang et al. 2008).

4.2 Physical processes connecting ENSO Modoki to winter climate over the Pacific and its rim

4.2.1 Air–sea feedback and associated zonal circulation change

Large-scale circulation variation and further climate change can be induced by the anomalous air–sea interaction

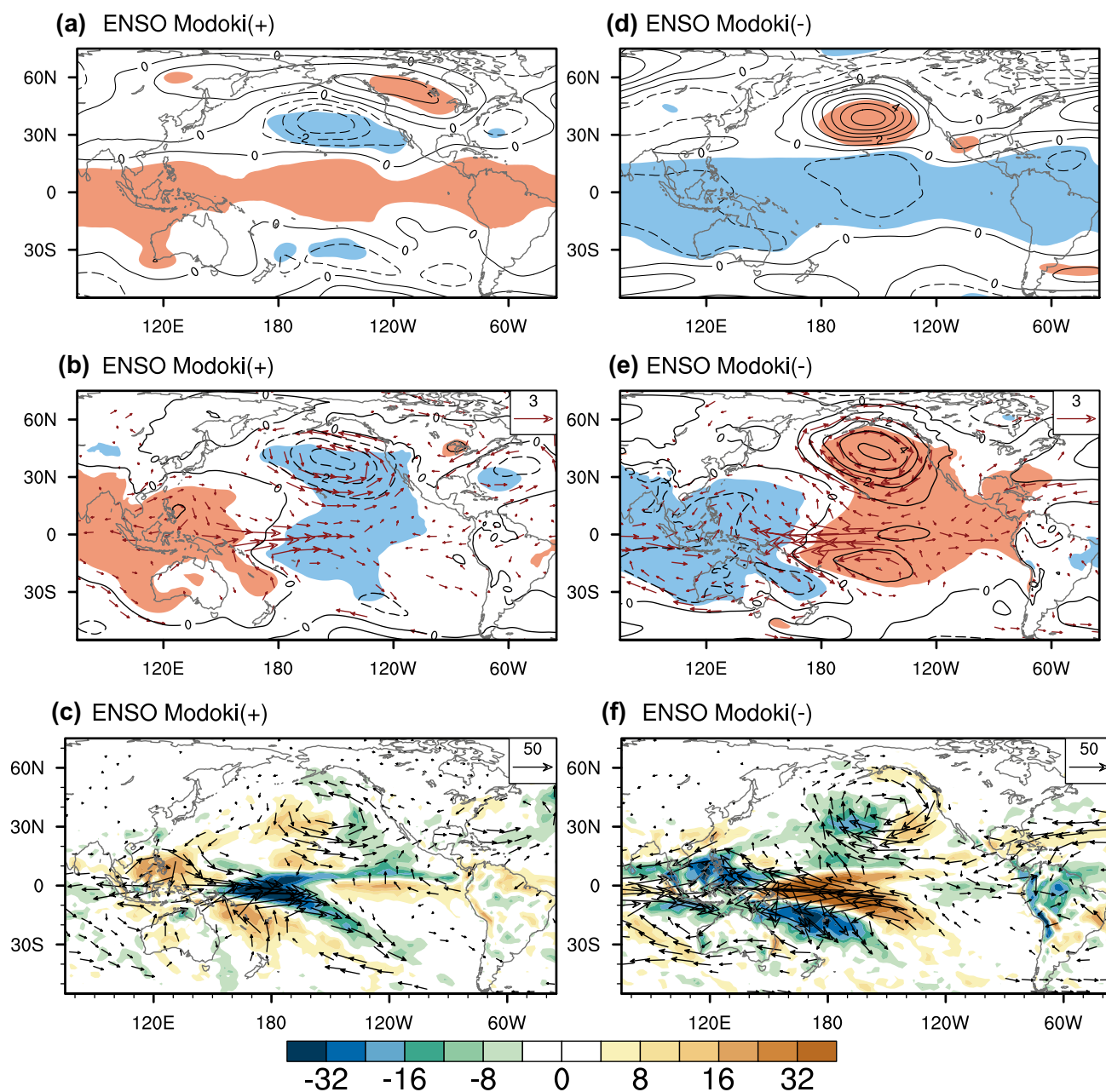


Fig. 5 Composite DJF 500 hPa geopotential height (**a, b**, contour, unit: gpm), 850 hPa wind (**c, d**, vector, unit: m s^{-1}) and SLP (**c, d**, contour, interval: 1 hPa), and vertically integrated WVf (**e, f**, vector, unit: $\text{kg (m s}^{-1})$) and its divergence (shading, unit: 10^{-6} kg (m^2

$\text{s}^{-1})$ anomalies during 1979–2017. Only significant vectors are plotted. Salmon (blue) shading denotes 90% confident level for positive (negative) anomalies from a Student's t test

(Philander et al. 1984). Previous studies have generally explored the dynamic and thermodynamic feedbacks in the Pacific Ocean (Cayan 1992a, b; Hendon and Glick 1997). Recently, Marathe et al. (2015) quantitatively compared the intensity of the dynamic and thermodynamic feedbacks by surface wind forcing, SST anomalies, thermocline variation, and heat flux during the two flavors of El Niño, and found that the proposed El Niño Modoki is distinctly different from the canonical El Niño. In this study, the composites of

300 hPa velocity potential, 300 hPa divergent wind, and 500 hPa vertical velocity are calculated for the analysis of the dynamical process during ENSO Modoki events (Fig. 7). In addition, we investigate the change in surface heat flux and surface net radiation to discuss the thermodynamic feedback during ENSO Modoki events. These can reveal the zonal circulation change and related air–sea interaction caused by the zonal thermodynamic difference. Owing to surface sensible heat flux (SHF) anomalies and surface net longwave

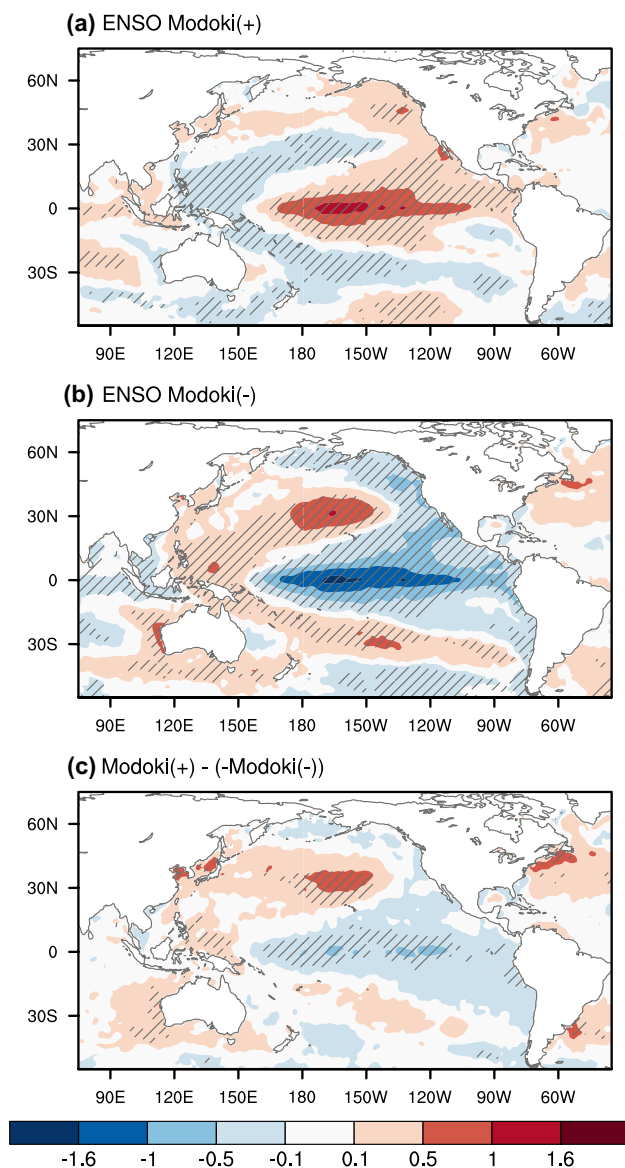


Fig. 6 The same as Fig. 3, but for SST anomalies from the HadISST dataset

radiation (LWR) anomalies being far less than the surface latent heat flux (LHF) anomalies and surface net shortwave radiation (SWR) anomalies, we only provide LHF and SWR anomalies here (Fig. 8).

As shown in Fig. 7a, upper-level velocity potential and divergent wind anomalies are characterized by a tripolar pattern over the tropical Pacific during El Niño Modoki boreal winter (Weng et al. 2009; Feng et al. 2010), that is, anomalous divergence (ascending) is centered in the central equatorial Pacific and anomalous convergence (descending) is located over both sides (Fig. 7a,c), in line with changes in the SST (Fig. 6). This implies that there are obvious changes in the Walker circulation under the thermodynamic activity.

During El Niño Modoki winter, a “boomerang” pattern of anomalous upper-level divergence is observed over the Pacific Ocean, which encompasses strong centers in the northeastern Pacific and central equatorial Pacific and a weak one centered at 10° S, 120° W (Fig. 7a), reducing the SLP over these regions (Fig. 4c). Thus, anomalous cyclonic winds (Fig. 8a) and ascending motion (Fig. 7c) occur, which dynamically favors winter precipitation (Fig. 3e). Furthermore, warm SST anomalies (Fig. 6a) enhance evaporation and release more LH into the atmosphere in the central and eastern equatorial Pacific (Fig. 8c), resulting in more rainy days (Fig. 4a) and less SWR received by the sea surface (Fig. 8e) over there. Notably, the position of the center of the upward LHF anomalies (Fig. 8c) is eastward compared with the center of warm SST anomalies over the central equatorial Pacific (Fig. 6a). This results from the contrary role of surface wind anomalies over the central-eastern and central-western equatorial Pacific (Fig. 8a) associated with the Walker circulation change. Over the western equatorial Pacific, anomalous upper-level convergence is centered and extends to most regions of East Asia, Southeast Asia, and northwestern Australia. Thus, the corresponding positive SLP and descending anomalies suppress the rainfall and favor downward SWR, especially over the Maritime Continent. Meanwhile, cold SST anomalies over the western equatorial Pacific inhibiting the upward LHF, which also contributes to the drying.

In the extratropical North Pacific, anomalous cyclonic winds occur in the lower troposphere (Fig. 8a). A decrease in the sea–air temperature and humidity difference caused by warm and wet airflow (Fig. 8a) along the western North American coast suppresses the upward LHF, and further drives local warm SST anomalies (Fig. 6a). Near the Bering Sea, decreased surface winds inhibit the LHF from the ocean to the atmosphere, and moisture is transported by the anomalous northeasterly winds to low latitudes and thus WV divergence is formed there, leading to dry anomalies. Therefore, under the air–sea interaction, winter precipitation anomalies are characterized by a pattern of positive east and negative west in the mid–high latitudes of the North Pacific. In addition, anomalous cyclonic winds and climate impacts observed over the tropical South Pacific, which is basically symmetrical with the North Pacific, are far less than anomalies over the North Pacific. On land, anomalies of descending (Fig. 7c) and downward SWR (Fig. 8e) lead to a warmer summer over western Australia, and northwestern and northern South America (Fig. 3a).

During La Niña Modoki, anomalous upper-level convergence (Fig. 7b) forced by cold SST anomalies over the central equatorial Pacific (Fig. 6b) extends to the North American continent and extratropical eastern South Pacific, leading to a stronger dry “boomerang” pattern over the Pacific Ocean (Fig. 4b). On both sides of the equatorial

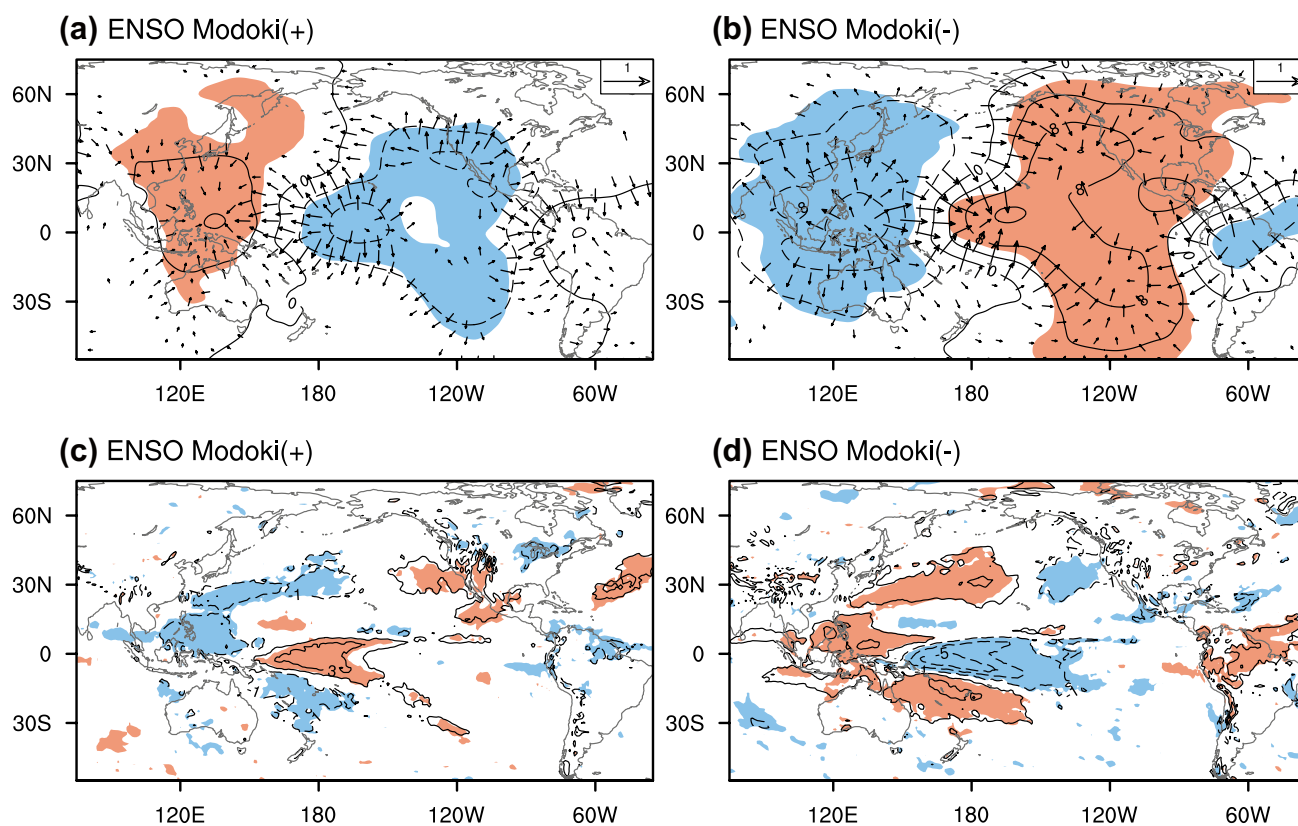


Fig. 7 The same as Fig. 5a, b, but for 300 hPa divergent winds (**a**, **b**, vector, unit: m s^{-1}), velocity potential (**a**, **b**, contour, interval: $4 \times 10^5 \text{m}^2 \text{s}^{-1}$), and 500 hPa vertical velocity (**c**, **d**, contour, interval: 10^{-2}m s^{-1}) anomalies

Pacific, the intensified divergence anomalies are accompanied by strong ascending motion (Fig. 7d), causing wet anomalies over the northern Maritime Continent and northern South America. Meanwhile, the opposite and intensified widespread anomalies of surface wind (Fig. 8b), surface heat flux (Fig. 8d,f), and SST induce a strong tropical air–sea interaction, which also contributes to the stronger boreal winter climate change over the tropical Pacific Rim compared with El Niño Modoki.

4.2.2 Local-mean meridional circulation change

Beyond differences in zonal thermodynamic, the SST anomalies during ENSO Modoki could also reform the meridional thermodynamic gradient. Baines (2006) revealed that the mass and moisture transported by local meridional circulation are essential to the distribution of precipitation. Figure 9 shows the composites of the average of $100^\circ \text{E} - 270^\circ \text{E}$ regional meridional circulation anomalies. During El Niño Modoki winter, the alternating zonal wind anomalies dominate the Northern Hemisphere, and its variation corresponds to a “negative–positive–negative” pattern of 500 hPa geopotential height anomalies (Fig. 5a). Ascending anomalies caused by positive SST anomalies (Fig. 6a)

are observed around the Equator and 40°N in the troposphere, and sinking motion is mainly seen in the low-latitude Pacific (Fig. 9a). Another obvious sinking branch is around $45^\circ \text{N} - 60^\circ \text{N}$, related to the warm and dry anomalies in the northern mid-latitudes (Figs. 3a and 4a). Compared with El Niño Modoki, La Niña Modoki events occur with stronger anomalous meridional circulation and zonal wind in the tropical Pacific and weaker anomalies in the extratropical Pacific (Fig. 9b). Its descending anomalies are located at the Equator and ascending anomalies occur around $15^\circ \text{S} - 25^\circ \text{S}$ and $10^\circ \text{N} - 30^\circ \text{N}$, which extends from the surface to the stratosphere, suggesting that the deep system occurred in La Niña Modoki boreal winter. In other words, differences in the intensity and position of meridional circulation anomalies may also contribute to the asymmetry of precipitation anomalies in the Pacific.

5 Model experiment results

In this section, we further investigate the role of ENSO Modoki in the asymmetric climate anomalies during boreal winter using numerical experiments. Under the ENSO Modoki scenario, climate features are generally

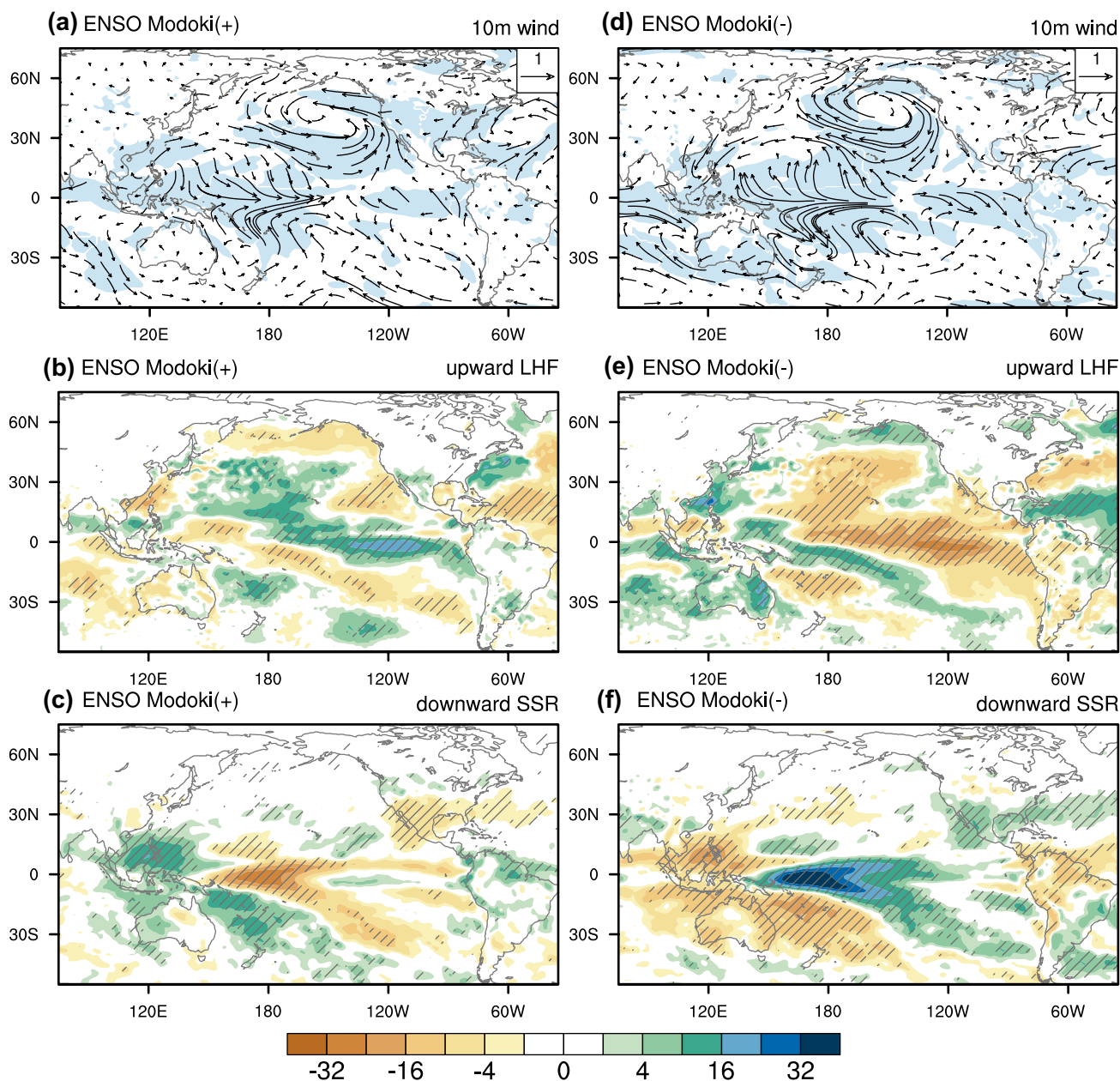


Fig. 8 Composite DJF 10 m wind (**a, b**, vector, unit: m s^{-1}), upward surface LHF (**c, d**, contour, unit: W m^{-2}), and downward SWR (**e, f**, contour, unit: W m^{-2}) anomalies during El Niño Modoki (left panel)

and La Niña Modoki (right panel). Shading (**a, b**) and Slant hatching (**c–f**) denote the 90% confident level from a Student’s *t* test

reproduced by the model, including the tripolar pattern of SAT (Fig. 10a, b) and rainfall anomalies (Fig. 10d, e) over the tropical Pacific Ocean, the dipolar pattern of rainfall anomalies over the extratropical Pacific Ocean, and several aspects of SAT and rainfall anomalies on land. The simulated composite difference between El Niño Modoki and La Niña Modoki (Fig. 10c) shows that stronger SAT anomalies occurred over the western coast of the United States, northeastern South America, and northeastern Australia (eastern United States) during La Niña Modoki (El Niño

Modoki) as observed (Fig. 3c). However, the asymmetry in the simulation over southwestern Australia and South China is opposite to the observational results. As for simulated precipitation anomalies, the composite difference (Fig. 10f) shows stronger anomalies over the Bering Sea, southeastern United States, northeastern South America, northeastern Australia, and the Bay of Bengal (western coast of United States) during La Niña Modoki (El Niño Modoki), which is consistent with the observational results

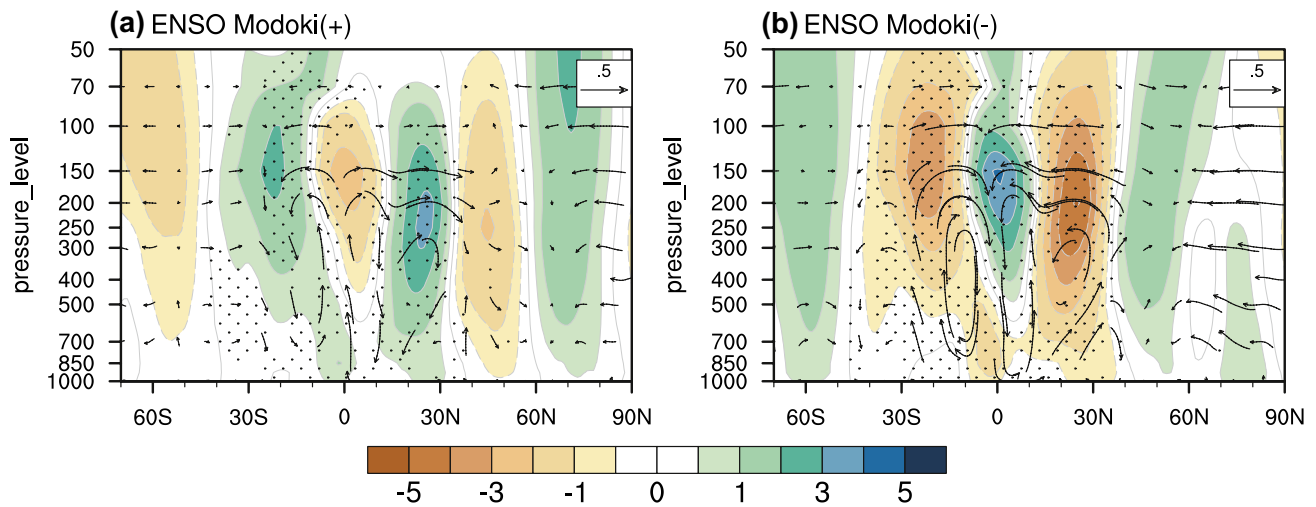


Fig. 9 Composite of DJF $100^{\circ}E - 270^{\circ}E$ average of Hadley circulation anomalies (vector, units: $m s^{-1}$) and zonal wind anomalies (shading, units: $m s^{-1}$) during El Niño Modoki (a) and La Niña Modoki

(b). The vertical velocity anomalies are multiplied by -100 . Vectors with dots denote the 90% confident level from a Student's t -test

(Fig. 4c), but the experiments miss the asymmetry in the Philippines and tropical central–eastern Indian Ocean.

Furthermore, we examine the different response of the atmospheric circulation in the simulations. During El Niño Modoki (Fig. 11a–c), anomalous ascending (descending) motion occurs with the upper-level divergence (convergence) and lower-level convergence (divergence) over the tropical central Pacific (both sides), which is basically opposite in La Niña Modoki (Fig. 11d–f). In the extratropics, a stronger PNA teleconnection is simulated during El Niño Modoki (Fig. 11b) compared with La Niña Modoki (Fig. 11e). These features in the numerical experiments coincide well with the observations (Figs. 5 and 7), but details in the Okhotsk Sea during El Niño Modoki are opposite to the observational results, and the greater intensity of circulation anomalies over tropical Pacific during La Niña Modoki is not obvious compared with the observational results. In addition, strong regional meridional circulation anomalies in the tropical South Pacific with the La Niña Modoki forcing (Fig. 12b) are consistent with the observations (Fig. 9b), while the simulated results during El Niño Modoki are more robust than observed, especially in the northern high latitudes (Fig. 12a). In summary, the numerical simulations basically reproduce the asymmetric characteristics of the observed climate anomalies and associated atmospheric circulation change over most areas, but show dissimilar features in some regions, particularly in East Asia.

6 Summary and discussion

In this paper, we study the teleconnection between ENSO Modoki events and boreal winter climate anomalies over the Pacific and its rim. Composite analysis reveals that the

relationship between ENSO Modoki and climate—the SAT and precipitation—is asymmetric in position and intensity during boreal winter. The results show that warm anomalies are detected over most regions of the tropical Pacific Rim during El Niño Modoki, which is opposite but intensified in La Niña Modoki, especially in the western Marine Continent, northeastern Australia, and northern South America. Notably, a zonal tripolar pattern with “positive–negative–positive” anomalies occur in Australia during El Niño Modoki (Fig. 3a), whereas a meridional dipolar pattern with “positive–negative” anomalies is observed in La Niña Modoki (Fig. 3b). For rainfall anomalies, ENSO Modoki occurs with multiple “boomerang” patterns over the Pacific Ocean and it is stronger during La Niña Modoki. On land, a decrease in rainfall occurs in the northern Maritime Continent, northern South America, and southwestern Australia during El Niño Modoki, which is reversed but enhanced in La Niña Modoki. Moreover, a dipolar pattern of wet and dry conditions in the southern and northern United States is detected only in El Niño Modoki, while drying in southwestern China and the Gulf Coast, and wetting in northeastern Australia and Venezuela are observed only during La Niña Modoki.

The asymmetry is related to different changes in the air–sea feedback and large-scale dynamical processes during ENSO Modoki events. In El Niño Modoki boreal winter, the “positive–negative–positive” pattern of upper-level divergence and WVF divergence anomalies dominate the tropical Pacific, accompanied by the multifaceted effects of the “negative–positive” pattern of LHF anomalies, which causes precipitation anomalies involving the northern Marine Continent, western Australia, and northeastern South America. Meanwhile, a PNA-like pattern is forced

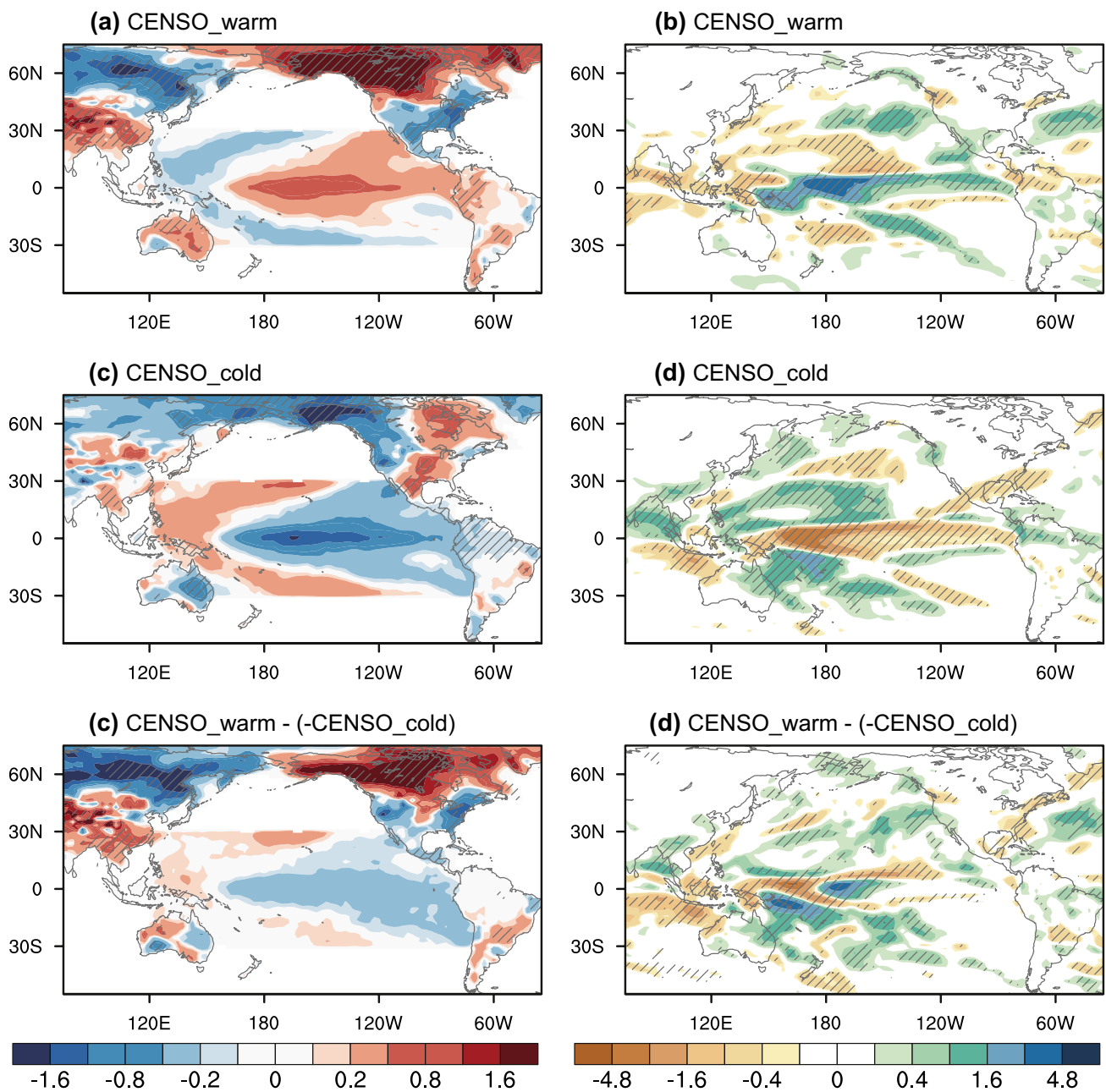


Fig. 10 The same as Figs. 3a, b and 4a, b, but for simulated SAT and precipitation anomalies, respectively

by warm SST anomalies over the central equatorial Pacific, which contributes to the dipolar pattern of wet south and dry north in the United States. This implies a robust interaction between the tropics and extratropics in El Niño Modoki events. However, during La Niña Modoki, under the opposite and enhanced changes in atmospheric circulation and WVF, stronger anomalies are observed in the Pacific Ocean and over tropical land, but fewer impacts over mid-latitude North America.

Meanwhile, to examine the asymmetric climate response to same intensity of SST anomaly during El

Niño Modoki and La Niña Modoki winter, we conducted two additional numerical experiments with the opposite ENSO Modoki SST anomalies (Table S1). The results show that climate anomalies forced by El Niño Modoki and opposite El Niño Modoki are asymmetric (Fig. S2), which is similar to the features in Fig. 10. Similar asymmetric can also be observed in the climate response by opposite La Niña Modoki and La Niña Modoki (Fig. S3). It implies that boreal winter climate anomalies during different phases of ENSO Modoki are asymmetric even with the same SST anomaly intensity, and the observed stronger

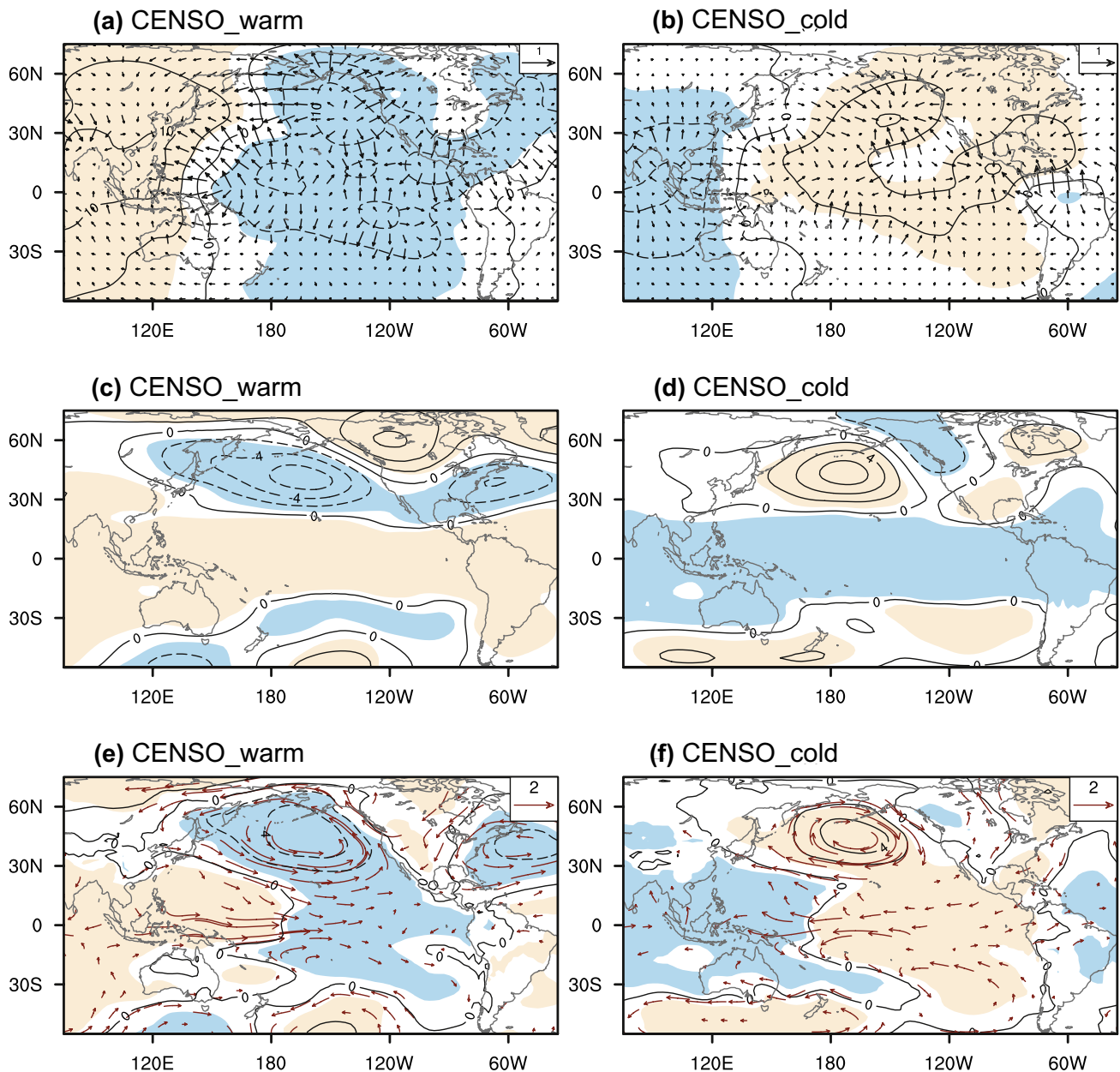


Fig. 11 The same as Fig. 7, but for simulated 300 hPa divergent winds (**a, b**), velocity potential (**a, b**, interval: $5 \times 10^5 m^2 s^{-1}$), 500 hPa geopotential height (**c, d**, interval: 2gpm), 850 hPa wind (**c, d**, unit:

$m s^{-1}$), and SLP (**e, f**, interval: 2 hPa) anomalies. Light salmon (blue) shading denotes 90% confident level for positive (negative) anomalies from a Student's *t* test

SST anomalies during La Niña Modoki could aggravate this asymmetry.

Furthermore, the observed signal is captured by numerical experiments. To some extent, the results imply that the asymmetric impacts of ENSO Modoki events on winter climate over the Pacific and its rim are due to the ENSO Modoki SST anomalies. However, some details in the mid-high latitudes are missing in the model, especially in East Asia. For example, opposite rainfall anomalies to the observations are simulated over the Yangtze River Basin

during different phases, and strong cold anomalies on the east of Lake Baikal is forced by El Niño Modoki, while warm anomalies are observed. The main source of the difference may come from the following points. On the one hand, SST anomalies over the Indian Ocean may affect the East Asian winter monsoon, and further have impacts on climate change over eastern China (Guo et al. 2017; Zou and Zhou 2017), but we consider only the SST anomalies over tropical Pacific Ocean. On the other hand, Cheng et al. (2019) consider that the ocean heat budget with regards to

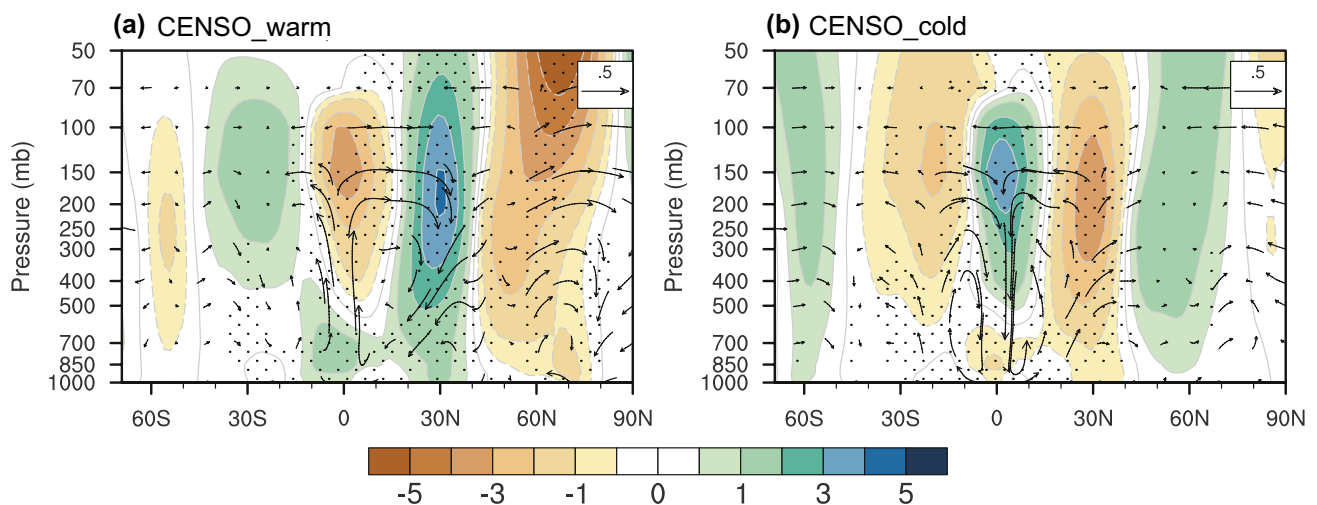


Fig. 12 The same as Fig. 9, but for simulated Hadley circulation (vector) and zonal wind (shading) anomalies

the asymmetry of ENSO remains to be verified due to insufficient observational data. In other words, SAT anomalies in the mid–high latitudes induced by the SST over the tropical Pacific are still in doubt in the model.

Acknowledgements This work was supported by the National Science Foundation of China (Grant Nos. 41421004) and the Startup Foundation for Introducing Talent of NUIST (No. 2243141801031). All the datasets can be accessed publicly. The NCEP analysis dataset can be downloaded from <https://www.esrl.noaa.gov/psd/data>.

References

- Adler R et al (2018) The global precipitation climatology project (GPCP) monthly analysis (New Version 2.3) and a review of 2017 global precipitation. *Atmosphere* 9:138. <https://doi.org/10.3390/atmos9040138>
- Ashok K, Behera SK, Rao SA, Weng HY, Yamagata T (2007) El Niño Modoki and its possible teleconnection. *J Geophys Res Oceans*. <https://doi.org/10.1029/2006jc003798>
- Baines PG (2006) The zonal structure of the Hadley circulation. *Adv Atmos Sci* 23:869–883. <https://doi.org/10.1007/s00376-006-0869-5>
- Battisti DS, Hirst AC (1989) Interannual variability in a tropical atmosphere–ocean model: influence of the basic state, ocean geometry and nonlinearity. *J Atmos Sci* 46:1687–1712. [https://doi.org/10.1175/1520-0469\(1989\)046<1687:IVIATA>2.0.CO;2](https://doi.org/10.1175/1520-0469(1989)046<1687:IVIATA>2.0.CO;2)
- Berrisford P, Dee D, Poli P, Brugge R et al (2011) The ERA-Interim archive: version 2.0. ERA Report Series 1:23
- Bjerknes J (1969) Atmospheric teleconnections from the equatorial Pacific. *Mon Weather Rev* 97:163–172. [https://doi.org/10.1175/1520-0493\(1969\)097<0163:ATFTEP>2.3.CO;2](https://doi.org/10.1175/1520-0493(1969)097<0163:ATFTEP>2.3.CO;2)
- Brönnimann S (2007) Impact of El Niño–southern oscillation on European climate. *Rev Geophys*. <https://doi.org/10.1029/2006RG000199>
- Cai WJ, van Rensch P, Cowan T, Sullivan A (2010) Asymmetry in ENSO teleconnection with regional rainfall, its multidecadal variability, and impact. *J Clim* 23:4944–4955. <https://doi.org/10.1175/2010jcli3501.1>
- Cayan DR (1992a) Latent and sensible heat-flux anomalies over the northern oceans—driving the sea-surface temperature. *J Phys Oceanogr* 22:859–881. [https://doi.org/10.1175/1520-0485\(1992\)022<0859:Lashfa>2.0.CO;2](https://doi.org/10.1175/1520-0485(1992)022<0859:Lashfa>2.0.CO;2)
- Cayan DR (1992b) Latent and sensible heat-flux anomalies over the northern oceans—the connection to monthly atmospheric circulation. *J Clim* 5:354–369. [https://doi.org/10.1175/1520-0442\(1992\)005<0354:Lashfa>2.0.CO;2](https://doi.org/10.1175/1520-0442(1992)005<0354:Lashfa>2.0.CO;2)
- Cheng LJ, Trenberth KE, Fasullo JT, Mayer M, Balmaseda M, Zhu J (2019) Evolution of ocean heat content related to ENSO. *J Clim* 32:3529–3556. <https://doi.org/10.1175/Jcli-D-18-0607.1>
- Feng JA, Wang L, Chen W, Fong SK, Leong KC (2010) Different impacts of two types of Pacific Ocean warming on Southeast Asian rainfall during boreal winter. *J Geophys Res-Atmos*. <https://doi.org/10.1029/2010jd014761>
- Feng J, Chen W, Tam CY, Zhou W (2011) Different impacts of El Niño and El Niño modoki on China rainfall in the decaying phases. *Int J Climatol* 31:2091–2101. <https://doi.org/10.1002/joc.2217>
- Freund MB, Henley BJ, Karoly DJ, McGregor HV, Abram NJ, Dommenget D (2019) Higher frequency of Central Pacific El Niño events in recent decades relative to past centuries. *Nat Geosci* 12:450. <https://doi.org/10.1038/s41561-019-0353-3>
- Gent PR et al (2011) The community climate system model version 4. *J Clim* 24:4973–4991. <https://doi.org/10.1175/2011jcli4083.1>
- Guo Z, Zhou T, Wu B (2017) The asymmetric effects of El Niño and La Niña on the East Asian winter monsoon and their simulation by CMIP5 atmospheric models. *J Meteorol Res* 31:82–93. <https://doi.org/10.1007/s13351-017-6095-5>
- Hao X, He SP (2017) Combined effect of ENSO-like and atlantic multidecadal oscillation SSTs on the interannual variability of the east asian winter monsoon. *J Clim* 30:2697–2716. <https://doi.org/10.1175/Jcli-D-16-0118.1>
- Harris IC, Jones PD (2015) CRU TS3.23: climatic research unit (CRU) time-series (TS) version 3.23 of high resolution gridded data of month-by-month variation in climate (Jan. 1901–Dec. 2014). Centre Environ Data Anal. <https://doi.org/10.5285/4c7fd6fa-f176-4c58-acee-683d5e9d2ed5>
- Hendon HH, Glick J (1997) Intraseasonal air–sea interaction in the tropical Indian and Pacific Oceans. *J Clim* 10:647–661. [https://doi.org/10.1175/1520-0442\(1997\)010<0647:Iasiii>2.0.CO;2](https://doi.org/10.1175/1520-0442(1997)010<0647:Iasiii>2.0.CO;2)

- Jadhav J, Panickal S, Marathe S, Ashok K (2015) On the possible cause of distinct El Niño types in the recent decades. *Sci Rep* 5:17009. <https://doi.org/10.1038/srep17009>
- Jin FF (1997a) An equatorial ocean recharge paradigm for ENSO. Part I: conceptual model. *J Atmos Sci* 54:811–829. [https://doi.org/10.1175/1520-0469\(1997\)054<0811:Aeorpf>2.0.Co;2](https://doi.org/10.1175/1520-0469(1997)054<0811:Aeorpf>2.0.Co;2)
- Jin FF (1997b) An equatorial ocean recharge paradigm for ENSO. Part II: a stripped-down coupled model. *J Atmos Sci* 54:830–847. [https://doi.org/10.1175/1520-0469\(1997\)054<0830:Aeorpf>2.0.Co;2](https://doi.org/10.1175/1520-0469(1997)054<0830:Aeorpf>2.0.Co;2)
- Kao HY, Yu JY (2009) Contrasting eastern-pacific and central-pacific types of ENSO. *J Clim* 22:615–632. <https://doi.org/10.1175/2008jcli2309.1>
- Karori MA, Li JP, Jin FF (2013) The asymmetric influence of the two types of el nino and la nina on summer rainfall over South-east China. *J Clim* 26:4567–4582. <https://doi.org/10.1175/Jcli-D-12-00324.1>
- Kim DW, Choi KS, Byun HR (2012) Effects of El Niño Modoki on winter precipitation in Korea. *Clim Dyn* 38:1313–1324. <https://doi.org/10.1007/s00382-011-1114-1>
- Kug JS, Jin FF, An SI (2009) Two types of el nino events: cold tongue el nino and warm pool el nino. *J Clim* 22:1499–1515. <https://doi.org/10.1175/2008jcli2624.1>
- Marathe S, Ashok K, Swapna P, Sabin TP (2015) Revisiting El Niño Modokis. *Clim Dyn* 45:3527–3545. <https://doi.org/10.1007/s00382-015-2555-8>
- Mariotti A (2007) How ENSO impacts precipitation in southwest central Asia. *Geophys Res Lett*. <https://doi.org/10.1029/2007gl030078>
- Philander SGH, Yamagata T, Pacanowski RC (1984) Unstable air sea interactions in the tropics. *J Atmos Sci* 41:604–613. [https://doi.org/10.1175/1520-0469\(1984\)041<0604:Uasiit>2.0.Co;2](https://doi.org/10.1175/1520-0469(1984)041<0604:Uasiit>2.0.Co;2)
- Preethi B, Sabin TP, Adedoyin JA, Ashok K (2015) Impacts of the ENSO Modoki and other tropical Indo-Pacific climate-drivers on African rainfall. *Sci Rep* 5:16653. <https://doi.org/10.1038/srep20266>
- Rayner NA et al (2003) Global analyses of sea surface temperature, sea ice, and night marine air temperature since the late nineteenth century. *J Geophys Res Atmos*. <https://doi.org/10.1029/2002jd002670>
- Salimun E, Tangang F, Juneng L, Behera SK, Yu WD (2014) Differential impacts of conventional El Niño versus El Niño Modoki on Malaysian rainfall anomaly during winter monsoon. *Int J Climatol* 34:2763–2774. <https://doi.org/10.1002/joc.3873>
- Samir Cordoba-Machado S, Palomino-Lemus R, Gamiz-Fortis SR, Castro-Diez Y, Esteban-Parra MJ (2015) Assessing the impact of El Niño Modoki on seasonal precipitation in Colombia. *Global Planet Change* 124:41–61. <https://doi.org/10.1016/j.gloplacha.2014.11.003>
- Screen JA (2014) Arctic amplification decreases temperature variance in northern mid- to high-latitudes. *Nat Clim Change* 4:577–582. <https://doi.org/10.1038/Nclimate2268>
- Suarez MJ, Schopf PS (1988) A delayed action oscillator for ENSO. *J Atmos Sci* 45:3283–3287. [https://doi.org/10.1175/1520-0469\(1988\)045<3283:Adaofe>2.0.Co;2](https://doi.org/10.1175/1520-0469(1988)045<3283:Adaofe>2.0.Co;2)
- Sun B, Zhu YL, Wang HJ (2011) The recent interdecadal and interannual variation of water vapor transport over eastern China. *Adv Atmos Sci* 28:1039–1048. <https://doi.org/10.1007/s00376-010-0093-1>
- Tedeschi RG, Cavalcanti IFA, Grimm AM (2013) Influences of two types of ENSO on South American precipitation. *Int J Climatol* 33:1382–1400. <https://doi.org/10.1002/joc.3519>
- Wang B, Yang J, Zhou T, Wang B (2008) Interdecadal changes in the major modes of Asian–Australian monsoon variability: strengthening relationship with ENSO since the late 1970s. *J Clim* 21:1771–1789. <https://doi.org/10.1175/2007jcli1981.1>
- Wang Z, Zhang W, Geng X (2017) Different influences of two types of ENSO on winter temperature and cold extremes in northern China. *Acta Meteorologica Sinica* 75:564–580. <https://doi.org/10.11676/qxxb2017.038> (in Chinese)
- Weng HY, Ashok K, Behera S, Rao AS, Yamagata T (2007) Impacts of recent El Niño Modoki on dry/wet conditions in the Pacific rim during boreal summer. *Clim Dyn* 29:113–129. <https://doi.org/10.1007/s00382-007-0234-0>
- Weng H, Behera SK, Yamagata T (2009) Anomalous winter climate conditions in the Pacific rim during recent El Niño Modoki and El Niño events. *Clim Dyn* 32:663–674. <https://doi.org/10.1007/s00382-008-0394-6>
- Wyrtki K (1975) El Niño—the dynamic response of the equatorial Pacific Ocean to atmospheric forcing. *J Phys Oceanogr* 5:572–584. [https://doi.org/10.1175/1520-0485\(1975\)005<0572:ENTDR O>2.0.CO;2](https://doi.org/10.1175/1520-0485(1975)005<0572:ENTDR O>2.0.CO;2)
- Xu W, Ma J, Wang W (2005) A review of studies on the influence of ENSO events on the climate in China. *Sci Meteorol Sinica* 25:212–220 (in Chinese)
- Yu JY, Kim ST (2011) Relationships between extratropical sea level pressure variations and the central Pacific and eastern Pacific types of ENSO. *J Clim* 24:708–720. <https://doi.org/10.1175/2010jcli3688.1>
- Yu JY, Kao HY, Lee T (2010) Subtropics-related interannual sea surface temperature variability in the central equatorial Pacific. *J Clim* 23:2869–2884. <https://doi.org/10.1175/2010jcli3171.1>
- Yu LJ, Zhong SY, Heilman WE, Bian XD (2017) A comparison of the effects of El Niño and El Niño Modoki on subdaily extreme precipitation occurrences across the contiguous USA. *J Geophys Res Atmos* 122:7401–7415. <https://doi.org/10.1002/2017jd026683>
- Zhang WJ, Li JP, Jin FF (2009) Spatial and temporal features of ENSO meridional scales. *Geophys Res Lett*. <https://doi.org/10.1029/2009gl038672>
- Zhang WJ, Jin FF, Zhao JX, Li JP (2013) On the Bias in Simulated ENSO SSTA meridional widths of CMIP3 models. *J Clim* 26:3173–3186. <https://doi.org/10.1175/Jcli-D-12-00347.1>
- Zou L, Zhou T (2017) Dynamical downscaling of East Asian winter monsoon changes with a regional ocean–atmosphere coupled model. *Quart J R Meteorol Soc* 143:2245–2259. <https://doi.org/10.1002/qj.3082>

Publisher's Note Springer Nature remains neutral with regard to jurisdictional claims in published maps and institutional affiliations.